Comparison of Different Bipolar Construct Configurations for the Correction of Adult Spine Deformity: A Finite Element Analysis

Claudio Vergari[1] · Sylvain Persohn[1] · Stéphane Wolff[2] · Pierre-Emmanuel Moreau[2] · Lotfi Miladi[3] · Guillaume Riouallon[2]

Abstract

Purpose A minimally invasive bipolar spinal fixation was recently developed to correct the deformity in pediatric neuromuscular scoliosis and has recently been adapted for adult scoliosis. Although the clinical results are promising, mechanical complications are still not negligible. In this work, alternative configurations of bipolar constructs were compared through numerical simulation, in order to evaluate stress distribution along the implant according to each configuration.

Methods The configurations included doubling the rods, adding lumbar screws to strengthen the distal anchorage, and combining two different materials (titanium and chromium-cobalt alloy). This resulted in seven different configurations, which were implemented in a subject-specific and experimentally validated finite element model, based on the geometry of an asymptomatic subject. Von Mises stresses were compared between configurations.

Results The results confirm that doubling the rods reduced mid-rod stresses, as expected, but also shifted some of the load from the distal anchorage to the rods, which is a common site of implant failure. The addition of pedicle screws also reduced the stress in the distal anchorage. The configuration showing the best compromise between stress reduction and the mini-invasive character of surgery included a doubling of both rods in titanium.

Conclusions These results should be confirmed by clinical results, but they already provide clear guidelines for the surgeon.

Keywords Minimally invasive · Finite element model · Neuromuscular scoliosis · Fusion-less surgery · Iliosacral screws · Bipolar technique

Introduction

Spine fusion is the most common technique to treat adult spine deformity, although between 13 and 30% of patients can still suffer from complications [1–3]. In particular, mechanical complications are the most common, and they represent up to 67% of total complications, while systemic, neurological, and infectious complications can represent 47% [4]. Among mechanical complications, a recent literature review by Akıntürk et al. reported 17.1% of proximal junctional kyphosis, 13.5% of rod/screw breakage, 11.1% screw loosening, and 2.6% distal junctional kyphosis.

A minimally invasive approach has been developed that requires only two short incisions in the upper thoracic spine and at the lumbosacral junction for proximal and distal anchorage points, aiming to reduce the complication rates while still achieving delayed spinal fusion after progressive ankylosing of the spine [5]. This bipolar construct was initially developed for pediatric cases, and it was recently adapted to adults [6]. Mechanical and infectious complication rates of bipolar constructs were similar to or lower than those occurring with arthrodesis, especially when compared to traditional growing rods in the pediatric population [7]. Recent results of bipolar constructs in adult patients showed satisfactory curve correction (40%), with

Associate Editor Elisabetta Zanetti oversaw the review of this article.

✉ Claudio Vergari
c.vergari@gmail.com

[1] Arts et Métiers Institute of Technology, EPF Engineering School, Université Sorbonne Paris Nord, IBHGC–Institut de Biomécanique Humaine Georges Charpak, F-75013 Paris, France

[2] Department of Orthopedic Surgery, Paris Saint-Joseph Hospital Group, Paris, France

[3] Pediatric Orthopedic Surgery Department, Necker University Hospital, APHP, University of Paris-Cité, Paris, France

14.6% of infections and 23% mechanical complications 9 months postoperatively [8].

While promising, these results suggest that the method could be improved, particularly in terms of mechanical complications. The lumbosacral region seems to be more affected, with rod breakages and problems related to the connector of iliosacral screws [6, 8]. Concerning rod fracture, different constructs may be able to reduce this complication rate while maintaining the minimally invasive approach of this technique. In particular, rods can be doubled to share the load, a complementary iliosacral screw in S2 or pedicle screws can be added in the lumbar region to protect or to reinforce the iliosacral anchorage, and different materials can be used. For example, chromium-cobalt (CrCo) is stiffer than the commonly used titanium, and the former is sometimes preferred to achieve greater curve correction [9, 10], so the combination of these materials could improve patient outcomes.

However, clinical studies cannot go further in comparing different constructs because of ethical and patient safety considerations. For this reason, finite element modeling has been used for a long time to test innovative implant designs [11, 12], and beam-based models allow to combine the fast computation time of such mathematical implementation with the accurate reproduction of patient-specific geometry and kinematics. Such models have often been used to study spinal implants and bracing [13–18]. In particular, a patient-specific model was developed and used for the simulation of spine surgery [19, 20], after being experimentally validated for the simulation of bipolar constructs [21].

In this study, different configurations of the bipolar construct for adult deformity were compared in terms of rod stress and residual spinal range of motion. The aim was to determine which configurations are more promising for further clinical applications, with the longer-term objective of reducing mechanical complications with bipolar constructs.

Methods

Participant

One healthy male subject (62 years old) who was included in previous studies [22] (after approval of the ethical committee CPP Ile-de-France VI 6036) was retrospectively included in the present work. He underwent standing biplanar radiography (Fig. 1).

Finite Element Model

A 3D reconstruction of the subject's spine, rib cage, and pelvis was performed using methods that were previously validated in terms of geometrical accuracy and reproducibility [23–25]. His full spinal length was 43.1 cm (from T1 to L5). A subject-specific finite element model was then built from this geometry, as previously described [26], to obtain a numerical model characterized by realistic intervertebral mobility and fast computational time. Vertebral bodies, intervertebral discs, posterior elements (pedicles, spinous and transverse processes), pelvis, sternum, ribs, and costovertebral joints were modeled as beam elements. Figure 2 shows an example of the model at the L3 level; the model does not include a volume mesh but beam.

Rib cartilage and articular facets were modeled as shell elements, and articular joints were modeled as frictionless contacts of deformable surfaces, with a normalized contact stiffness of 1300 force/length [27]. Ligaments (interspinal, supraspinal, intertransverse, flavum, ilio-lumbar,

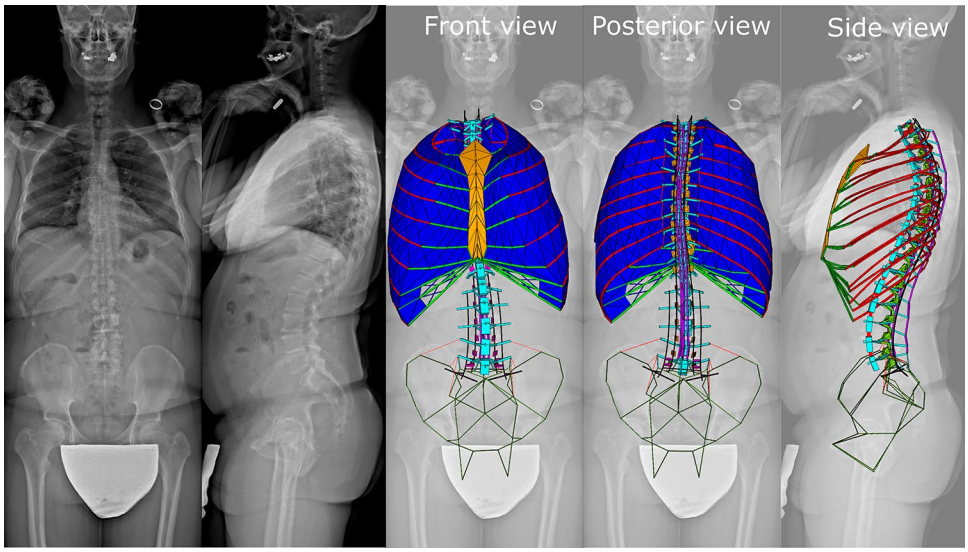

Fig. 1 Biplanar radiography of a 62-year-old male asymptomatic subject, and subject-specific finite element model. The bipolar instrumentation (configuration 1) is represented in black. The intercostal cartilage and ligaments have been hidden in the side view for clarity

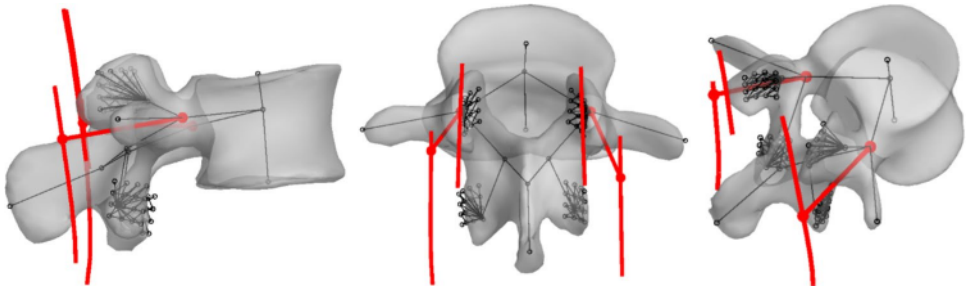

Fig. 2 Finite element model of the L3 vertebra, including the rods running posteriorly and the pedicle screws. All vertebral elements are modeled as beams, as well as the rods and screws. The volumetric vertebra is obtained through the 3D reconstruction of the subject's spine, and it is used to calculate the positions of the beam nodes, while the finite element model does not include volume mesh

costovertebral, and intercostal ligaments) were modeled as cables with nonlinear mechanical properties, i.e., with a stress–strain relationship including a toe region and a linear region, which were calibrated based on experimental data [27]. Intervertebral discs were also modeled as beams, and their mechanical behavior was approximated with third-degree polynomials, which were normalized on each disc height and second moment of area [21]. Discs' mechanical properties were different in each loading direction (compression, flexion extension, lateral bending, torsion) to realistically reproduce intervertebral kinematics. Mechanical properties of all elements are listed in Table 1, while the complete model is shown in Fig. 1.

The model was previously validated against experimental data [21]: briefly, five cadaveric lumbar segments (L1 to S1) and six thoracic segments (C6 to T7) were tested by applying pure moments in three directions (flexion extension, lateral bending, and torsion) to determine the experimental spinal range of motion. The samples were then instrumented with arthrodesis, which was equipped with a strain gauge on one rod, and tested again. Then, the FEM was used to simulate the same loading on an additional *in vivo* spinal geometry, which did not belong to the experimental batch, and the results showed that the simulated spinal range of motion fell within the experimental one, both with and without spinal implant, and rod strain was the same between experiment and simulation (0.013 vs 0.010%, respectively, or 130 vs. 100 microstrain). The mechanical properties of the spinal segments that were not included in the experimental campaign (T8–T12) were extrapolated from the available data (i.e., the stiffness of the available levels and the geometrical properties of the missing ones).

The boundary conditions were as follows: the pelvis was fixed, and pure moments of 5 Nm were applied to T1 vertebra in flexion/extension, right and left bending, right and left torsion. This loading is also consistent with the range that was attained in the experimental validation of the thoracic spinal segments [21]. A schematic view of the boundary conditions is provided in Fig. 3.

Simulations were performed on the intact spine, and then with different variants of bipolar instrumentation, as described below. The model was implemented in Ansys

Table 1 Mechanical properties of the finite element model

Structure	Element type	Elastic modulus (MPa)	Poisson's ratio
Vertebral bodies	Beam	1000 [28]	0.3
Intervertebral discs	Beam	Third degree polynomial relationship between moment and rotation [21]	0.45
Pedicles, posterior arches, apophysis	Beam	5000 [28]	0.3
Spinous and transverse processes	Beam	3500 [28]	0.3
Articular facets	Shell	5000 [28]	0.3
Sternum	Beam	10000 [28]	0.2
Ribs	Beam	2790–7440 [29, 30]	0.1
Costovertebral joints	Beam	5-50 [31]	0.2
Costal cartilage	Shell	480 [28]	0.1
Ligaments	Cable	Multilinear [27]	0.2
Ti-6Al-4 V rods and connectors	Beam	110000	0.3
CrCo rods and connectors	Beam	220000	0.3

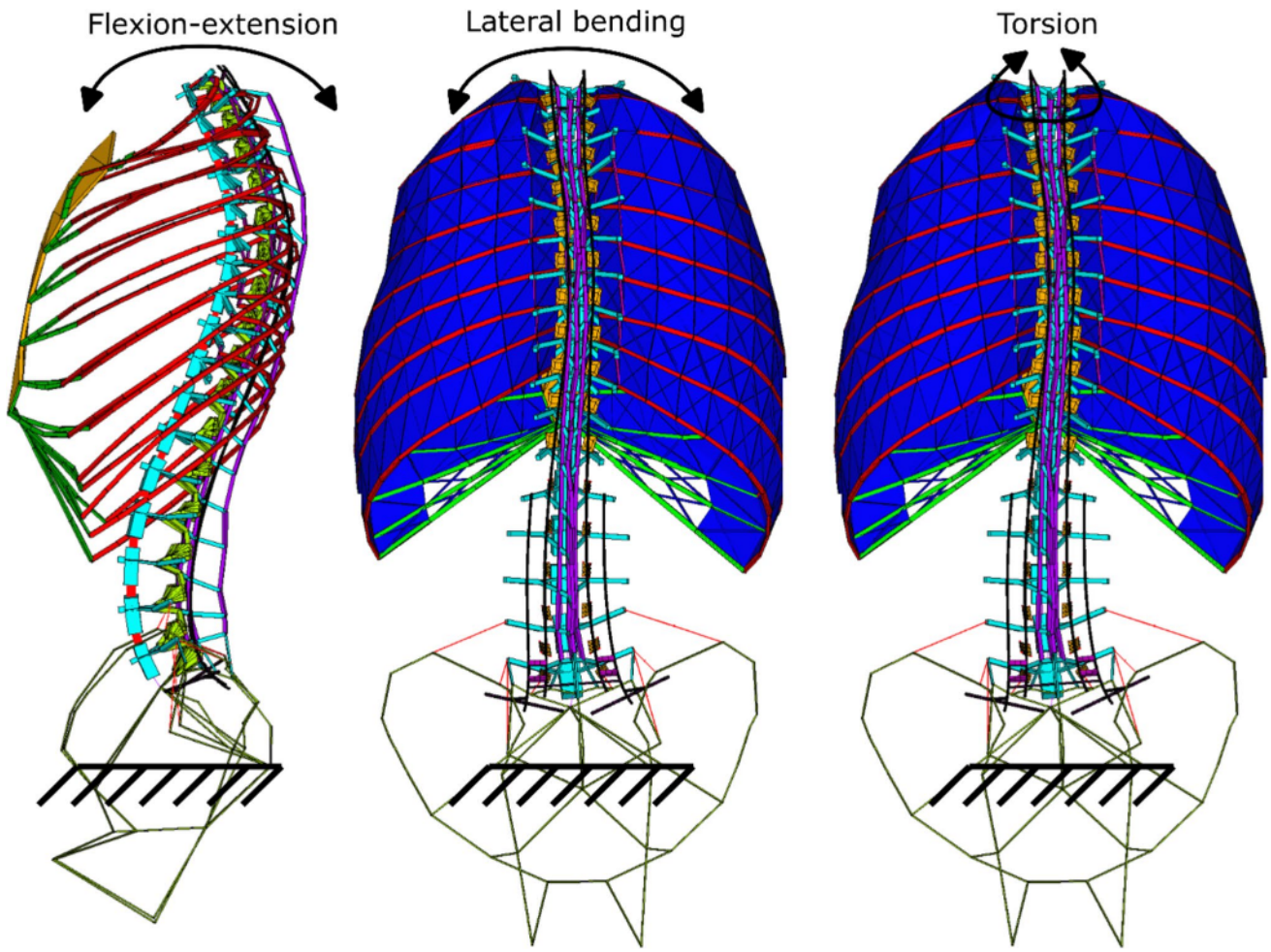

Fig. 3 Schematic view of the boundary conditions

V2023 (Ansys Inc, Canonsburg, Pennsylvania, United States).

Bipolar Construct Configuration

The bipolar fusionless construct is characterized by two proximal double hook claws consisting of supralaminar and pedicle hooks fixed on two adjacent vertebrae (T1–T2 and T4–T5), a cross-link at T3, two pre-curved rods (5.5 mm diameter) attached to two shorter lateral rods that are fixed to a distal connector at L5 (E.SPINE TANIT® Iliosacral fixation, EUROS SAS, France). Two iliosacral screws fix the construct to the pelvis, while three cross-links stabilize the system [5].

Three geometrical configurations were compared in the present work. Configuration 1 is the base configuration as described above (Fig. 4), with two rods linking the proximal and distal anchoring. In configuration 2, the lateral rods, which were structurally functional only up to the L5 level in the previously published works, were prolonged cranially and attached to the medial rods at the T4–T5 level. In configuration 3, the lateral rods were attached to the medial ones at L2, and pedicle screws were added at L3, L4, and L5.

In the base configuration, all rods were in titanium (Ti-6Al-4 V), and this variant was named "1TT," where the number represents the configuration, and the first and second letters represent the material of the lateral and medial rods, respectively (Fig. 4). A variation of this configuration was considered, where the medial rods were in CrCo alloy (1TC, Fig. 4). Two variants of the base configuration 2 (2TT) were also considered: one with all rods in CrCo alloy (2CC) and one with only the medial rods in CrCo alloy (2TC). Finally, a variant of configuration 3 (3TT) was considered, in which the medial rods were made of CrCo alloy (3TC).

In the model, the rods were implemented using beam elements (BEAM188), as well as the transverse connectors, iliosacral and pedicle screws. The connectors between the rods were modeled as a beam with a rectangular section. Screws were rigidly attached to the rods and bone nodes (pelvis or pedicles). Titanium and CrCo alloy were considered as

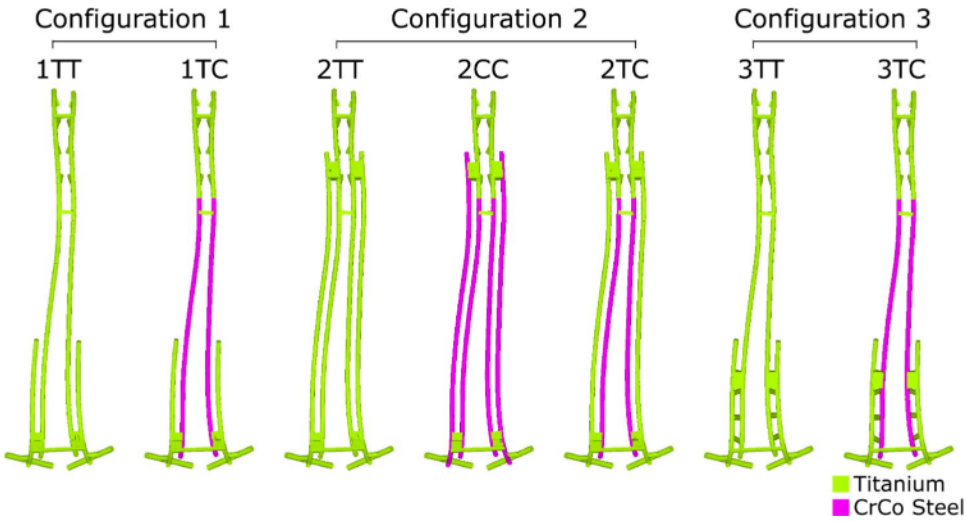

Fig. 4 Configurations and variants of the bipolar instrumentations. Each variant is represented by the configuration number followed by the initial of the lateral and medial rod material. For instance, variant 2TC has the geometry of configuration 2 with lateral titanium rods and medial CrCo steel rods

linear materials with elastic moduli of 110 GPa and 220 GPa, respectively, and a Poisson's ratio of 0.3.

Analysis

Overall spinal range of motion was measured as changes in orientation and position of the T1 vertebra relative to the fixed pelvis, to estimate spinal range of motion reduction with the different constructs. Von Mises stresses were calculated in all rods and compared between variants, to estimate sites at risk of rupture.

Results

Mobility

Table 2 reports spinal range of motion in all configurations. Overall, rotations in the instrumented spines were reduced by 87% in flexion extension, 90% in lateral bending, and 73% in torsion when the spine was loaded with pure moments in the respective directions. Translations were reduced by 91% in flexion/extension, 94% in lateral bending, and 23% in torsion. The largest range of motion reduction was obtained by the 2CC variant (88% rotation and 93% translation reduction), while configuration 1TT obtained the largest range of motion (76% rotation and 83% translation reduction).

Rod Stress

Figure 5 shows the von Mises stress in all rods; left and right rods showed similar stresses, so they were averaged across all configurations.

The standard 1TT configuration showed the highest stress in the distal anchorage, which is consistent with the clinically observed material failures. Lateral bending and torsion also showed high stress in the rods.

In flexion/extension, doubling the rods allowed for a reduction of almost half the stress in the long rods, from 77 MPa in 1T to 42 MPa in 2TT (45% reduction) in extension, a 49% reduction in lateral bending (104.8 to 53 MPa), and a 35% reduction in torsion (from 106 to 69 MPa). The highest stress in medial rods was observed in the lumbar region of the 1TC variant (97 MPa), while the highest stress in the lateral rods was in the 2CC variant (150 MPa), at the level of the iliosacral screws. The 3TT and 3TC variants showed the lowest stresses. Mixing materials had a significant effect in these loading conditions: peak stress in the free rods was similar in the lateral and medial rods in 2TT (42 vs 40 MPa) and in 2CC (49 vs 46 MPa), but much different in 2TC: 31 MPa in the lateral titanium rod vs. 58 MPa in the medial CoCr rod (46% difference).

In left/right bending, all configurations showed relatively uniform stress all along the free part of the medial rods, but again the 1TC variant showed the highest values, while the 2TT variant showed the lowest. Stresses in the lateral rods were lower in 3TT, where the load was shared with the pedicle screws. It must be noticed that the peak stress shifted to the lumbosacral junction in configuration 2, while for configuration 3, it was transferred above the lumbar pedicle screws and was similar to configuration 1 in the proximal long rod.

In left/right torsion, again all configurations showed relatively uniform stress, with 1TC showing the highest values and 2TT the lowest. Configurations 1 and 2 showed higher stress in the lateral rod than configuration 3. Again, in this last configuration, the peak stress shifted above the pedicle screws in the long single rod. Configuration 2TC also showed an effect of mixing material, with a 50% difference in stress between the lateral titanium rod (40 MPa) and the medial CrCo rod (79 MPa).

Table 2 Spinal range of motion (measured as rotation and translation of T1 and L1 vertebrae relative to the fixed pelvis)

	Intact	1TT	1TC	2TT	2CC	2TC	3TT	3TC
T1 rotations [°]								
Flexion	31.0	4.3	3.8	3.8	3.4	3.6	2.6	2.6
Extension	28.4	5.6	4.8	4.8	4.1	4.4	2.5	2.5
Left bending	33.3	5.4	3.7	2.6	2.0	2.3	3.6	2.7
Right bending	34.0	5.7	3.8	2.6	2.0	2.3	3.6	2.8
Left torsion	29.7	12.3	8.7	8.4	5.8	6.9	9.6	7.4
Right torsion	32.3	12.5	8.7	8.4	5.8	6.9	9.6	7.4
T1 total 3D translation [mm]								
Flexion	151.7	16.5	13.8	13.8	11.6	12.8	5.6	5.2
Extension	141.1	24.8	20.2	20.3	16.2	18.5	5.6	5.2
Left bending	155.4	18.8	11.1	6.7	4.0	5.5	9.0	5.9
Right bending	156.8	19.9	11.4	6.8	4.0	5.5	9.2	5.9
Left torsion	14.2	13.3	8.5	9.2	5.6	7.0	13.2	8.7
Right torsion	10.8	13.6	8.5	9.2	5.6	7.0	13.3	8.7
L1 rotations [°]								
Flexion	18.5	0.9	0.7	0.7	0.6	0.7	0.0	0.0
Extension	15.8	1.2	0.8	0.9	0.6	0.8	0.0	0.1
Left bending	15.8	1.3	0.7	0.5	0.2	0.4	0.3	0.0
Right bending	16.3	1.4	0.7	0.5	0.2	0.4	0.3	0.0
Left torsion	8.0	4.0	2.8	2.8	1.7	2.1	1.4	1.3
Right torsion	9.2	4.4	2.9	2.8	1.7	2.2	1.4	1.3
L1 total 3D translation [mm]								
Flexion	28.6	5.2	4.4	4.5	3.9	4.2	0.7	0.6
Extension	32.3	8.2	6.9	7.0	5.6	6.4	0.7	0.7
Left bending	24.9	1.2	0.4	0.5	0.2	0.4	0.1	0.2
Right bending	27.2	1.7	0.6	0.7	0.2	0.4	0.2	0.2
Left torsion	3.6	5.2	3.8	3.3	2.1	2.7	2.0	1.5
Right torsion	7.4	5.5	3.9	3.3	2.1	2.7	1.9	1.5

For each loading, only the absolute rotation about the appropriate axis is reported (lateral axis for flexion/extension, posteroanterior axis for side bending, vertical axis for torsion). A reminder of the loading directions is provided in Figure 3

Discussion

The aim of this work was to compare different configurations and variants of a bipolar construct for spinal instrumentation using numerical simulation. All configurations allow to maintain the minimally invasive character of the procedure, needing only a distal and proximal incision. The pedicle screws required in configuration 3 can also be placed through the distal incision. Finite element modeling has been widely used to test innovative spinal implants and help surgeons decide their surgical strategy, provided the model is experimentally validated [32]. The subject-specific finite element model used in this work was previously validated against experimental data for the simulation of spinal instrumentations, both in terms of the intact spinal range of motion and in terms of rod strain in the instrumented spine [21]. Besides, a further validation is provided by the comparison of the numerical results with the clinical outcome. Hence, this model allowed to reproduce spine kinematic and mechanical behavior in full-range motions, with or without spinal implants, and to estimate implant stresses, which are risk factors for the bipolar construct.

The simulation of the base configuration (1TT) showed the highest stress in the distal anchorage, which is consistent with the material failures observed in clinical practice. Stress in the proximal anchorage was much lower than in the distal one in all loading directions, although stress in lateral bending and torsion was high in the rods.

Yield stress of Ti-6Al-4V alloy is 840 MPa, while it is closer to 650 MPa for CrCo alloy [33]. The maximal stress observed in titanium rods was 127 MPa (in the 2TT variant in torsion, lateral rod), while the maximal stress in CrCo was 150 MPa (in the 2CC variant in extension, lateral rod). Therefore, a significant safety margin is present, although these simulations only implement a static analysis, which should be consistent with physiological spinal loading. This does not take into account potential dynamic loads or shocks that the instrumented spine could undergo, nor

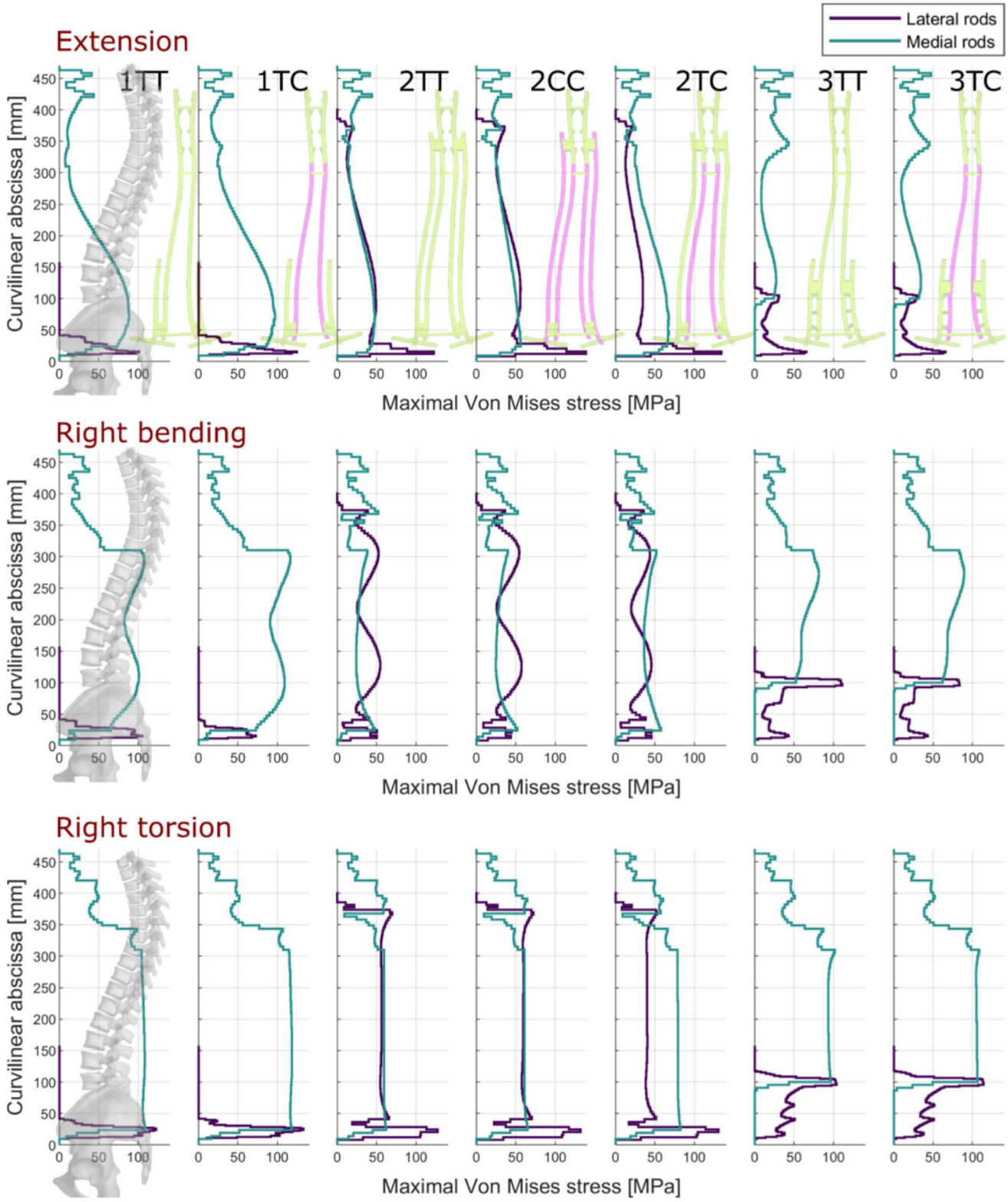

Fig. 5 Von Mises stress in all bipolar instrumentation variants. The curvilinear abscissa of 0 mm corresponds to the caudal end of the rods, while the maximum corresponds to the cranial end; the subject's 3D model is represented in one variant for reference. Stresses in left and right rods were averaged. For every direction of loading, only those showing highest stresses were plotted (extension, right bending, right torsion), because the stress distributions were very similar in the complementary direction

fatigue-related phenomena, which could have a significant impact on rod damage [34, 35]. Clinical studies have the final say on the damage mechanism of implant failure under physiological loading.

Results show that doubling the rods can lower the mid-rod stress, compared to the single-rod configurations, which is not surprising. Adding distal pedicle screws lowers the stress in the anchorage region, especially in flexion/extension. Hence, it appears that the base configuration, which was initially developed for neuromuscular scoliosis in children, could be improved in adult deformity by doubling the rods and strengthening the distal anchorage.

Reduction of range of motion in this study (between 73 and 94%, depending on construct and loading) was consistent with previous cadaveric tests on thoracic spines [36] and numerical modeling [21] (reductions between 68 and 98%). In general, a high reduction of range of motion is associated with better long-term fusion and avoiding pseudoarthrosis.

Mixing different materials showed a relatively small impact on the results, apart from the 2TC configuration, where the CrCo alloy rods are subjected to higher stress than the titanium rods in parallel, which is expected given the higher stiffness of the former. However, it was important to consider these material variations because CrCo alloy rods are often considered more adapted to obtain the initial spinal translation to correct the deformity, while the more compliant titanium rods are considered more adapted for their stress shielding of pedicle instrumentation [37]. The 2TT variant seems to represent the best compromise by attaining lower stress while preserving the mini-invasive character of the construct. In fact, 3TT requires more extensive lumbosacral access, from L2 to the sacrum, to place the pedicle screws. Furthermore, since the peak stress is more distal in the 2TT variant than in 3TT, the risk of loosening an iliosacral screw seems to be lower than that of a pedicle screw.

The main limitation of this work is that the anchorage points (proximal hooks and distal iliosacral screws) were simulated with a very simplified model. This approach does not allow to study in detail the interaction of the hooks with the vertebral posterior arch, but this does not represent an issue because this region is not at risk of failure (neither in the simulation nor in the clinical experience). However, the interaction between the screws and the pelvis cannot be finely studied either. This is a limitation because the sacral region could be at risk of failure, although the screw connector seems to be more affected than the bone–implant interface [6]. More detailed models exist which could be used to study more precisely this at-risk region and provide information on the failure mechanisms (screw pullout, connector failure, hook failure, etc.) [38].

The second limitation is that only an asymptomatic subject was studied. This was consistent with the aim of the present work, which is to compare different variants of the bipolar construct. A physiological but symmetrical subject geometry allowed to reduce the confounding effect of the subject's geometry. This also implies that potential effects of rod plasticization or preloading that occur during the translation of the spine were not accounted for. These aspects could significantly change the location of at-risk regions as well as the levels of maximum stress observed in the rods. This was also neglected in the present work to focus on the effects of the geometry of the bipolar construct: in fact, a scoliotic patient should have been considered to properly simulate rod plasticization and preloading, and this would have added another layer of complexity to the data analysis. However, the initial bending of the rods would have been similar in all configurations, so the impact on the comparison between them should be minimal. Nevertheless, further studies could aim to assess the effect of the deformity on the stresses induced on the instrumentation, including rod plasticization and preloading induced during surgery. Finally, gravitational and muscle loads were neglected, as is often the case in such comparative studies.

Conclusions

The present work has compared different variants of bipolar instrumentation using an experimentally validated finite element model. The results show that different choices regarding the geometric material properties of the construct can have a significant impact on the risk of implant failure and the residual range of motion of the spine. The results suggest that the original 1TT variant may not be the best option, since this variant leaves a relatively high degree of range of motion, while suffering from high stresses. In contrast, further clinical studies should focus on the 2TT and 3TT variants. 2TT strongly stabilizes the column with stress transfer to the lumbosacral junction, while 3TT also stabilizes the column in the lumbar region with stress transfer above the pedicle screws all along the long rod, to a level equivalent to that observed with the original construct (two rods) in bending and torsion. These results should now be compared with clinical results, but they can already guide future developments of bipolar instrumentation.

Author Contribution Claudio Vergari and Sylvain Persohn contributed toward design of the work, data interpretation, and drafting the work. Stéphane Wolff contributed toward data acquisition and manuscript reviewing. Stéphane Wolff and Pierre-Emmanuel Moreau contributed toward data acquisition and manuscript reviewing. Lotfi Miladi contributed toward data acquisition, data interpretation, and manuscript reviewing. Guillaume Riouallon contributed toward design of the work, data acquisition, data interpretation, and manuscript reviewing.

Funding The study was partially financed by EUROS Company.

Declarations

Competing interests The study was partially financed by EUROS Company. Lotfi Miladi reports a relationship with EUROS Company that includes: consulting or advisory. Guillaume Riouallon reports a relationship with Euros that includes: consulting or advisory, paid expert testimony, and travel reimbursement. Riouallon reports a relationship with Medtronic that includes: consulting or advisory and paid expert testimony.

Ethical Approval Patient data are from a previous study, which was approved by the ethical committee.

Clinical trial number Not applicable.

References

1. Akıntürk, N., M. Zileli, and O. Yaman. Complications of adult spinal deformity surgery: A literature review. *Journal of Craniovertebral Junction and Spine.* 13:17–26, 2022.
2. Riouallon, G., B. Bouyer, and S. Wolff. Risk of revision surgery for adult idiopathic scoliosis: a survival analysis of 517 cases over 25 years. *Eur Spine J*. 25:2527–2534, 2016.
3. Sansur, C. A., J. S. Smith, J. D. Coe, S. D. Glassman, S. H. Berven, D. W. Jr. Polly, J. H. Perra, O. Boachie-Adjei, and C. I. Shaffrey. Scoliosis research society morbidity and mortality of adult scoliosis surgery. *Spine* 36: 2011.
4. Smith, J. S., E. Klineberg, V. Lafage, C. I. Shaffrey, F. Schwab, R. Lafage, R. Hostin, G. M. Mundis, T. J. Errico, H. J. Kim, T. S. Protopsaltis, D. K. Hamilton, J. K. Scheer, A. Soroceanu, M. P. Kelly, B. Line, M. Gupta, V. Deviren, R. Hart, D. C. Burton, S. Bess, and C. P. Ames. Prospective multicenter assessment of perioperative and minimum 2-year postoperative complication rates associated with adult spinal deformity surgery. *J Neurosurg: Spine SPI*. 25:1–14, 2016.
5. Miladi, L., M. Gaume, N. Khouri, M. Johnson, V. Topouchian, and C. Glorion. Minimally invasive surgery for neuromuscular scoliosis: results and complications in a series of one hundred patients. *Spine*. 43:E968–E975, 2018.
6. Wolff, S., P.-E. Moreau, L. Miladi, and G. Riouallon. Is Minimally Invasive Bipolar Technique a Better Alternative to Long Fusion for Adult Neuromuscular Scoliosis? *Global Spine J*. 2023. https://doi.org/10.1177/21925682231159347.
7. Miladi, L., F. Solla, and M. Gaume. The minimally invasive bipolar fixation for pediatric spinal deformities: a narrative review. *Children* 11: 2024.
8. Wolff, S., K. Habboubi, A. Sebaaly, P. E. Moreau, L. Miladi, and G. Riouallon. Correction of adult spinal deformity with a minimally invasive fusionless bipolar construct: preliminary results. *Orthopaed Traumatol*. 105:1149–1155, 2019.
9. Etemadifar, M. R., A. Andalib, A. Rahimian, and S. M. H. T. Nodushan. Cobalt chromium-Titanium rods versus Titanium-Titanium rods for treatment of adolescent idiopathic scoliosis; which type of rod has better postoperative outcomes? *Rev. Assoc. Med. Bras.* 64:1085–1090, 2018.
10. Serhan, H., D. Mhatre, P. Newton, P. Giorgio, and P. Sturm. Would CoCr rods provide better correctional forces than stainless steel or titanium for rigid scoliosis curves? *J Spinal Disord Techniq*. 26:E70–E74, 2013.
11. Jain, P., M. Rana, J. K. Biswas, and M. R. Khan. Biomechanics of spinal implants—a review. *Biomed Phys Eng Express*. 6:042002, 2020.
12. Leszczynski, A., F. Meyer, Y.-P. Charles, C. Deck, N. Bourdet, and R. Willinger. Influence of double rods and interbody cages on range of motion and rod stress after spinopelvic instrumentation: a finite element study. *Eur Spine J*. 31:1515–1524, 2022.
13. Ali, A., V. Fontanari, W. Schmölz, and S. K. Agrawal. Active soft brace for scoliotic spine: a finite element study to evaluate in-brace correction. *Robotics*. 11:37, 2022.
14. Guy, A., H. Labelle, S. Barchi, E. Audet-Duchesne, N. Cobetto, S. Parent, M. Raison, and C. -É. Aubin. Braces designed using CAD/CAM combined or not with finite element modeling lead to effective treatment and quality of life after 2 years: a randomized controlled trial. *Spine*. 46:9, 2021.
15. Huynh, K. T., Z. Gao, I. Gibson, and W. F. Lu. Haptically integrated simulation of a finite element model of thoracolumbar spine combining offline biomechanical response analysis of intervertebral discs. *Comput-Aided Design*. 42:1151–1166, 2010.
16. Lafon, Y., V. Lafage, J. Dubousset, and W. Skalli. Intraoperative three-dimensional correction during rod rotation technique. *Spine*. 34:512–519, 2009.
17. Martin, S., N. Cobetto, A. N. Larson, and C.-E. Aubin. Biomechanical modeling and assessment of lumbar vertebral body tethering configurations. *Spine Deform*. 11:1041–1048, 2023.
18. Vergari, C., G. Ribes, B. Aubert, C. Adam, L. Miladi, B. Ilharreborde, K. Abelin-Genevois, P. Rouch, and W. Skalli. Evaluation of a patient-specific finite-element model to simulate conservative treatment in adolescent idiopathic scoliosis. *Spine Deformity*. 3:4–11, 2015.
19. Dumas, R., V. Lafage, Y. Lafon, J. P. Steib, D. Mitton, and W. Skalli. Finite element simulation of spinal deformities correction by in situ contouring technique. *Comput Methods Biomech Biomed Eng*. 8:331–337, 2005.
20. Lafon, Y., J.-P. Steib, and W. Skalli. Intraoperative three dimensional correction during in situ contouring surgery by using a numerical model. *Spine*. 35:453–459, 2010.
21. Vergari, C., M. Gaume, S. Persohn, L. Miladi, and W. Skalli. From in vitro evaluation of a finite element model of the spine to in silico comparison of spine instrumentations. *J Mech Behav Biomed Mater*. 2021. https://doi.org/10.1016/j.jmbbm.2021.104797.
22. Khalifé, M., W. Skalli, A. Assi, P. Guigui, V. Attali, R. Valentin, O. Gille, V. Lafage, H.-J. Kim, E. Ferrero, and C. Vergari. Sex-dependent evolution of whole-body postural alignment with age. *Eur Spine J*. 2024. https://doi.org/10.1007/s00586-024-08323-5.
23. Ghostine, B., C. Sauret, A. Assi, Z. Bakouny, N. Khalil, W. Skalli, and I. Ghanem. Influence of patient axial malpositioning on the trueness and precision of pelvic parameters obtained from 3D reconstructions based on biplanar radiographs. *European Radiology*. 27:1295–1302, 2017.
24. Humbert, L., J. A. De Guise, B. Aubert, B. Godbout, and W. Skalli. 3D reconstruction of the spine from biplanar X-rays using parametric models based on transversal and longitudinal inferences. *Med Eng Phys*. 31:681–687, 2009.
25. Vergari, C., B. Aubert, P. Lallemant-Dudek, T.-X. Haen, and W. Skalli. A novel method of anatomical landmark selection for rib cage 3D reconstruction from biplanar radiography. *Comput Methods Biomech Biomed Eng*. 8:15–23, 2020.
26. Vergari, C., I. Courtois, E. Ebermeyer, H. Bouloussa, R. Vialle, and W. Skalli. Experimental validation of a patient-specific model of orthotic action in adolescent idiopathic scoliosis. *Eur Spine J*. 25:3049–3055, 2016.
27. Chazal, J., A. Tanguy, M. Bourges, G. Gaurel, G. Escande, M. Guillot, and G. Vanneuville. Biomechanical properties of spinal ligaments and a histological study of the supraspinal ligament in traction. *Journal of Biomechanics*. 18:167–176, 1985.
28. Descrimes, J. L., C. E. Aubin, W. Skalli, R. Zeller, J. Danserau, and F. Lavaste. Introduction des facettes articulaires dans une

modélisation par éléments finis de la colonne vertébrale et du thorax scoliotique : aspects mécaniques. *Rachis*. 7:301–314, 1995.
29. Pezowicz, C., and M. Glowacki. The mechanical properties of human ribs in young adult. *Acta Bioeng Biomech*. 14:53–60, 2012.
30. Sandoz, B., A. Badina, S. Laporte, K. Lambot, D. Mitton, and W. Skalli. Quantitative geometric analysis of rib, costal cartilage and sternum from childhood to teenagehood. *Med Biol Eng Comput*. 51:971–979, 2013.
31. Lemosse, D., O. Le Rue, A. Diop, W. Skalli, P. Marec, and F. Lavaste. Characterization of the mechanical behaviour parameters of the costo-vertebral joint. *Eur Spine J*. 7:16–23, 1998.
32. Gould, S. L., L. Cristofolini, G. Davico, and M. Viceconti. Computational modelling of the scoliotic spine: a literature review. *Int J Numer Methods Biomed Eng*. 37:e3503, 2021.
33. Festas, A., A. Ramos, and J. Davim. Medical devices biomaterials—a review. *Proc Inst. Mech Eng, Part L: J Mater: Design Appl*. 234:218–228, 2020.
34. Natarajan, R. N., K. Watanabe, and K. Hasegawa. Posterior bone graft in lumbar spine surgery reduces the stress in the screw-rod system—a finite element study. *J Mech Behav Biomed Mater*. 104:103628, 2020.
35. Ribesse, A., K. Ismail, M. Croonenborghs, N. Irda, L. Miladi, P. J. Jacques, M. Mousny, and T. Pardoen. Fracture mechanisms in Ti and Co–Cr growing rods and impact on clinical practice. *J Mech Behav Biomed Mater*. 2021. https://doi.org/10.1016/j.jmbbm.2021.104620.
36. Gaume, M., S. Persohn, C. Vergari, C. Glorion, W. Skalli, and L. Miladi. Biomechanical cadaver study of proximal fixation in a minimally invasive bipolar construct. *Spine Deformity*. 8:33–80, 2020.
37. Warburton, A., S. J. Girdler, C. M. Mikhail, A. Ahn, and S. K. Cho. Biomaterials in Spinal Implants: A Review. *Neurospine*. 17:101–110, 2020.
38. Rana, M., J. K. Biswas, S. Roy, N. Ghosh, S. Bhattacharya, S. K. Karmakar, and A. Roychowdhury. Measurement of strain in the rod for lumbar pedicle screw fixation: an experimental and finite element study. *Biomed Phys Eng Exp*. 6:065035, 2020.
39. Panjabi, M. M. Hybrid multidirectional test method to evaluate spinal adjacent-level effects. *Clin Biomech*. 22:257–265, 2007.